Midinfrared picosecond spectroscopy studies of Auger recombination in InSb

V. Chazapis, H. A. Blom, K. L. Vodopyanov, A. G. Norman, and C. C. Phillips
Solid State Group, Physics Department, Imperial College of Science, Technology and Medicine, London SW7 2BZ, United Kingdom

(Received 19 January 1995; revised manuscript received 7 April 1995)

A midinfrared picosecond spectrometer based on an Er^{3+} laser-pumped optical parametric generator has been used to study Auger recombination processes in intrinsic InSb at room temperature. After carrier excitation by a 100-psec $\lambda=2.8$ μm Er^{3+} laser pulse the sample transmission change due to excess carriers was probed, using short pulses of wavelengths varying in the range 4–6 μm, as a function of time delay. It was shown that over the measured range of carrier densities ($n=10^{16}$–10^{18} cm^{-3}) the momentum-conserving conduction–heavy-hole–heavy-hole–light-hole Auger process was the predominant channel for electron-hole recombination with a quadratic rather than a cubic dependence of recombination rate on carrier density. The effective Auger lifetime scales as $\tau_{\mathrm{Aug}}^{-1}=C_2 n$ with $C_2=7.4(\pm 1.5)\times 10^{-9}$ cm^{3}s^{-1}. This type of carrier concentration dependence is in accordance with theoretical predictions for semiconductors in which the electron component of the carrier population is degenerate.

I. INTRODUCTION

Auger recombination (AR) is an intrinsic process that sets a fundamental limit to the radiative recombination efficiency in any optoelectronic device. In this process, an electron and a hole recombine and the resulting energy is transferred to a third carrier, either an electron or a hole. Typically the AR rate is determined by a "dominant channel," which (assuming parabolic bands) can be shown[1] to involve carriers with the following most probable energies:

$$E_1^{\mathrm{CCCH}}=E_2^{\mathrm{CCCH}}=\frac{m_c^2}{(2m_c+m_h)(m_c+m_h)}E_g \tag{1}$$

for electrons,

$$E_1'^{\mathrm{CCCH}}=\frac{m_c m_h}{(2m_c+m_h)(m_c+m_h)}E_g \tag{2}$$

for holes,

$$E_1^{\mathrm{CHHL}}=E_2^{\mathrm{CHHL}}=\frac{m_l m_h}{(2m_h+m_c)(2m_h-m_c-m_l)}E_g \tag{3}$$

for holes, and

$$E_1'^{\mathrm{CHHL}}=\frac{m_l m_c}{(2m_h+m_c)(2m_h+m_c-m_l)}E_g \tag{4}$$

for electrons, where m_c, m_h, and m_l are the carrier effective masses in the conduction (C), heavy (H), and light-hole (L) bands, respectively, E_g is the band-gap energy, and CCCH and CHHL denote the Auger-scattering events depicted in Fig. 1. E_1 plays the role of an effective energy barrier whose height is determined by carrier energy and momentum-conservation conditions, and this results in an exponential dependence of the AR rate on the temperature and the band-gap energy. For narrow-gap semiconductors, AR is a significant process at all but the lowest temperatures and carrier concentrations.

For semiconductor laser-diode applications the AR band-gap and temperature dependencies result in an empirical T_0 parameter for the laser threshold current density [$J_{\mathrm{th}} \propto \exp(T/T_0)$]. T_0 decreases with decreasing band gap from 160 to 200 K for $\lambda\approx 850$ nm GaAs/Al(GaAs) diode lasers to 50–60 K (Refs. 2 and 3) for $\lambda\approx 1.3$–1.5 μm (InGa)(AsP) lasers and to ≈ 17 K (Refs. 4 and 5) for $\lambda\approx 4$ μm In(AsSb) lasers. For infrared-detector applications, AR results in high generation-recombination diode currents. These give low zero-bias resistance-area products and low detectivities unless the detector is cooled and/or the carrier concentrations are reduced by the other means.[6]

Being a three-particle process, the AR rate is proportional to the integral over the carrier distributions of the product P of the occupation factors (Fig. 1) of the four participating states, which are linked by momentum and energy-conservation considerations:[7]

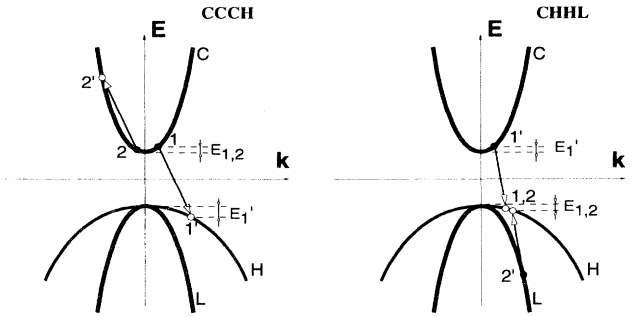

FIG. 1. Schematic representation of CCCH and CHHL Auger processes involving the "dominant channel" carriers of Ref. 12.

$$P^{\mathrm{CCCH}} \propto f_n(k_1) f_n(k_2) f_p(k_1') [1 - f_n(k_2')]$$

and (5)

$$P^{\mathrm{CHHL}} \propto f_p(k_1) f_p(k_2) f_n(k_1') [1 - f_p(k_2')] ,$$

where $f_{n(p)}$ represent electron (hole) occupation factors, respectively. The final term in Eq. (5), however, is typically unity, as the upper state 2′ is generally empty unless the carrier density is very high. If nondegenerate statistics apply, the integrals over the (Boltzmann) carrier distributions can be separated. In the limit of high excitation ($\Delta n \sim \Delta p \gg n_0, p_0$) the Boltzmann occupation probability in any given state is just proportional to the carrier density, and this gives a simple carrier-density dependence of the net AR rate, $dn/dt \propto n^2 p, p^2 n$ (i.e., $\propto n^3$ in the case here, where $n = p$), where n and p are the electron and hole concentrations. The effective Auger lifetime τ_{Aug} is then proportional to n^2, and can be written as $\tau_{\mathrm{Aug}}^{-1} = C_3 n^2$. This functional form has been verified and the value of the C_3 coefficient measured recently in InAs,[8] (InGa)As,[9] and in (InGa)(AsP) (Ref. 2) alloys.

In the case of InSb at 300 K, however, Eqs. (1)–(4) give (using the materials parameters of Table I) values for $E_{1,2}^{\mathrm{CCCH}}$, $E_{1,2}^{\mathrm{CHHL}}$, $E_1'^{\mathrm{CCCH}}$, and $E_1'^{\mathrm{CHHL}}$ all within a few meV of the conduction-band edge. Since even in ultrapure InSb the 300-K intrinsic Fermi energy is only ≈ 25 meV below this, the Boltzmann approximation fails at room temperature and this simple density-dependence approach is likely to fail even at arbitrarily low excess-carrier densities. At the carrier concentrations typically present (10^{16}–10^{18} cm^{-3}) in light-emitting and laser diodes the electron distribution is highly degenerate (although holes remain nondegenerate up to $p \approx 10^{18}$ cm^{-3}) and a full integration of the AR rate over the carrier distributions becomes necessary.

Haug[10] has studied the degenerate AR problem and concludes that, in the limit of high excess-carrier densities (i.e., $\Delta n, \Delta p \gg n_0, p_0$), negligible carrier screening, and a k-independent Auger-transition-matrix element, a $\tau_{\mathrm{Aug}}^{-1} \propto n$ dependence is expected. He also comments that the "normal" AR process is only likely to maintain its dominance into the degenerate regime if the band gap is small. In wide-gap materials, energy and momentum conservation considerations block the "normal" Auger interactions and higher-order processes (e.g., phonon-assisted and second-order AR) become significant.

Dutta and Nelson[2] consider the relative importance of these higher-order processes in (InGa)(AsP) alloys with band gaps corresponding to $\lambda \approx 1.3$–1.5 μm and find that, for $\Delta n \approx \Delta p \approx 10^{18}$ cm^{-3}, phonon-assisted AR processes are typically about an order of magnitude less probable than "normal" AR processes. The CCCH and CHHS "normal" processes are comparable in strength, and both roughly an order of magnitude more probable than the CHHL "normal" AR process (here S stands for split-off and L for light-hole band). The balance between the CCCH, CHHL, and CHHS rates is strongly sensitive to the band structure though, with, e.g., the CHHS rate dominating in GaSb (Ref. 11) due to an accidental near resonance between the fundamental and spin split-off band gaps. In InSb, however, the unusually large spin split-off energy ($\approx 4E_g$) renders the CHHS rate negligible, and we therefore conclude that the "normal" CCCH and CHHL processes will be dominant in the case of interest here. Beattie[12] has also suggested that these two processes should dominate in InSb and has calculated Auger constants taking into account Fermi-Dirac statistics, nonparabolic energy bands, and carrier screening effects. For 300-K intrinsic InSb, his calculations give (in the nondegenerate or "cubic" approximation when $dn/dt = -C_3 n^3$) $C_3 = 1.7 \times 10^{-26}$ cm^6 s^{-1} (CCCH process) and $C_3 = 1.2 \times 10^{-26}$ cm^6 s^{-1} (CHHL process), combining to give a total coefficient $C_3 = 2.9 \times 10^{-26}$ cm^6 s^{-1}.

Existing experimental data on AR rates in InSb are limited and to an extent contradictory. The recombination of an extremely high density ($n = 10^{19}$–10^{20} cm^{-3}) laser-induced electron-hole plasma in InSb at room temperature has been studied[13,14] using a plasma-reflection technique. The plasma was created with a 10-psec $\lambda = 1.06$ μm pulse, its reflectivity decay was probed with ultrashort 10.6-μm pulses, and an excess-carrier lifetime of 35 ± 5 psec for $n = 10^{19}$–10^{20} cm^{-3} was deduced. Modeling of the electron-hole plasma dynamics produced an AR coefficient for a "cubic" recombination rate dependence of $C_3 = 10^{-28}$ cm^6 s^{-1}—some two and half orders of magnitude smaller than predicted by Beattie.[12] A model with "quadratic" AR versus n dependence was more successful in describing the temporal evolution of the plasma reflectivity, however, and gave a best fit with $C_2 = 1.5 \times 10^{-9}$ cm^3 s^{-1}.

A similar method has also been used to study the decay of an InSb electron-hole plasma generated with nanosecond neodymium and ruby laser pulses.[15] The surface plasma density reached 6×10^{-18} cm^{-3} and gave a best-fit value for the "cubic" Auger recombination coefficient of $C_3 = 3 \times 10^{-27}$ cm^6 s^{-1}, although the "quadratic" functional relationship gave a better fit to the data and yielded $C_2 = 7.5 \times 10^{-9}$ cm^3 s^{-1}.

In these plasma-reflection experiments, noticeable reflection changes occur only when the dielectric function $\epsilon_r(\omega)$ approaches unity, which typically requires carrier densities $> 10^{18}$ cm^{-3} for the probe wavelengths available. The technique cannot be used at the lower carrier concentrations of interest for optoelectronic devices, and the carrier-recombination-rate values derived from these experiments depend on assumptions about transport conditions in the spatially nonuniform plasma. In practice, the carrier diffusion coefficients are density dependent, and this can create significant uncertainties in the modeling used to derive the Auger coefficients.

We here study the InSb AR rate as a function of carrier density using a time-resolved infrared pump-probe transmission spectroscopy technique applied to thin InSb films that have become available as a result of recent advances in molecular-beam-epitaxial growth. The method is essentially the same as used in previously reported[8] measurements in InAs thin films, but uses a different laser spectrometer to access the longer wavelengths required. The excess-carrier-density values created in our experiment (10^{16}–10^{18} cm^{-3}) are typical of those occurring in infrared emitter devices, and the more direct nature of the measurement technique allows us to identify the dom-

inant Auger mechanisms in this regime with significantly improved confidence.

II. EXPERIMENTAL METHOD

A mid-IR picosecond spectrometer based on an erbium laser pumping an optical parametric generator (OPG) was used for the pump-probe transmission measurements. Single 100-psec mode-locked pulses from an Er^{3+}:Cr^{3+}:YSGG laser ($\lambda=2.8$ μm, 3 Hz repetition rate) were amplified in a two-pass amplifier (Fig. 2) and part of the amplified pulse was used as a pump beam to create nonequilibrium carriers in the sample. The remaining portion was used to pump a traveling-wave double-pass OPG based on a 30-mm-long $ZnGeP_2$ nonlinear optical crystal.[16]

The OPG output pulses ($\sim$50 psec duration, 3.7 meV linewidth) were used to probe the sample transmission at varying delays after excitation. In all cases a sufficiently long delay was allowed, to ensure that the carrier distributions had thermalized to the lattice temperature and were spatially homogeneous. The probe wavelength could be tuned over the range $3.9<\lambda<10$ μm simply by rotating the OPG crystal in the plane of its z axis using a stepper motor. In this experiment we used three probing wavelengths: 4.16, 4.43, and 6.06 μm, corresponding to phonon energies 75%, 65%, and 20% above the InSb band gap, respectively.

The sample studied was an undoped 3.4-μm-thick InSb epilayer grown by molecular-beam epitaxy on a 0.5-mm-thick infrared-transparent semi-insulating GaAs substrate. It was mounted at Brewster's angle (76°) to eliminate interference effects from the Fresnel reflections at its surfaces, and all measurements were performed at room temperature. Figure 3 shows the small-signal absorption spectrum of the sample obtained with an IR spectrophotometer together with the positions of the pump and probe wavelengths.

The pump beam ($\lambda=2.8$ μm, $\hbar\omega\sim2.6E_g$) fluence at the sample surface was varied over the range 5–6500 μJ/cm^2 to create different initial nonequilibrium excess carrier concentrations. At the maximum pump fluence the InSb interband transitions were completely saturated,

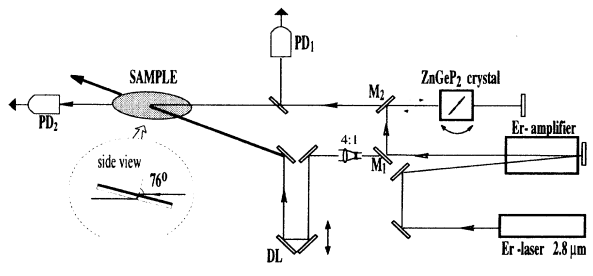

FIG. 2. Schematic of the tunable infrared picosecond spectroscopy system: PD_1 and PD_2, cooled cadmium mercury telluride photodiode detectors; M_1 and M_2, dielectric beamsplitters; DL, variable optical delay line.

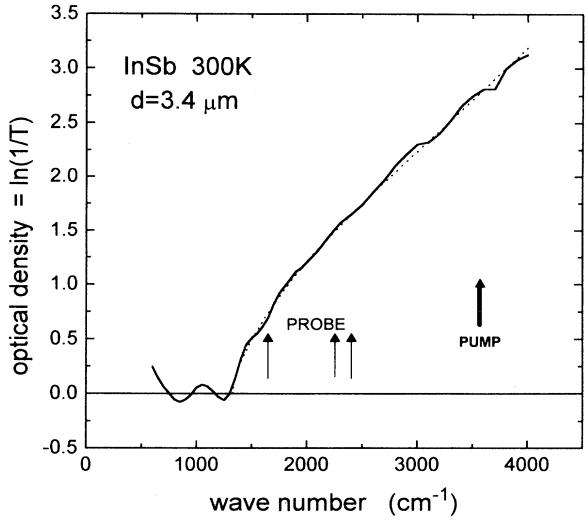

FIG. 3. Solid line, measured small signal absorption of the 3.4-μm-thick InSb sample at room temperature. The oscillatory structure at photon energies below the band gap is due to interference caused by Fresnel reflections at the InSb layer interfaces in this normal incidence measurement. Dotted line, absorption spectrum calculated with the three-band absorption model, using the conduction-band nonparabolicity parameters of Table I and assuming a k-independent optical matrix element for interband transitions.

corresponding to electron quasi-Fermi level $\approx$0.3 eV above the bottom of the conduction band and a carrier concentration of approximately 2.7×10^{18} cm^{-3}.

The probe pulse had much weaker fluence (<1 μJ/cm^2 at the sample surface) to ensure the absence of unwanted additional sample bleaching. Its diameter ($\sim$1 mm) was

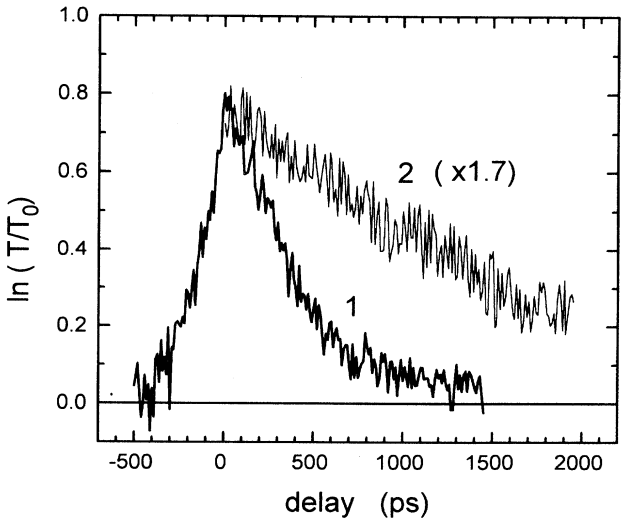

FIG. 4. Probe sample transmission T ratioed against the small-signal value T_0 as a function of pump-probe time delay: Solid line, probe wavelength $\lambda=4.16$ μm; dotted line, probe wavelength, $\lambda=6.06$ μm. Curve 2 is scaled up by a factor of 1.7 for clarity.

kept much smaller than that of the pump beam (~4 mm) to ensure uniform excitation density over the probed area, and Fig. 4 shows typical induced sample transmission (T) change transients plotted as $\ln(T/T_0)$ versus the time delay between the pump and probe pulses.

III. RESULTS

The main effect of the high excess photoexcited carrier concentration in InSb is an absorption decrease at photon energies above the band gap due to the dynamic Moss-Burstein effect. At these carrier densities the band-gap renormalization energy is negligible compared with the Moss-Burstein shift.

In order to convert the measured optical transmission change transients at a given probe wavelength to a carrier-concentration decay profile we consider interband absorption in a three-band model (with a nonparabolic conduction band), characterized by the parameters[17] of Table I. The conduction-band nonparabolicity parameter α was calculated semiempirically from a best fit to published electron effective mass versus electron concentration data.[17]

In contrast to previous similar measurements[8] in InAs and in InSb, light- to heavy-hole transitions and free-electron absorption are important and need to be taken into account in a quantitative analysis. This fact was immediately apparent in the experimental data from the fact that maximum achievable bleaching of the InSb layer (in terms of the optical density change) was only 50–70 % (compared with the 100% previously seen[8] in InAs), even at fluences close to the sample damage threshold. According to previous small-signal absorption measurements[18] made with doped samples in the 5–10 μm range, both these absorption mechanisms give an absorption coefficient component proportional to the excess-carrier concentration and are characterized by the cross sections $\sigma_p = 8.65\times10^{-16}$ cm^2/hole (independent of λ) and $\sigma_n = 0.23\times10^{-16}$ cm^2/electron at $\lambda = 9$ μm (proportional to λ^2). Thus the induced free-carrier absorption is dominated by light- to heavy-hole transitions in this case.

By modeling the maximum transmission change we observed at both the probe and pump wavelengths we derived our own free-carrier-induced absorption cross-section value of $\sigma = 1.56\times10^{-15}$ cm^2/carrier pair. This is roughly a factor of 2 larger but in broad agreement with the previously reported doped-sample data,[18] the discrepancy probably arising from the influence of ionized impurity scattering in the latter. From the point of view of the quantitative modeling, an error of a factor of 2 in the assumed free-carrier absorption cross-section affects our extracted carrier-concentration values by less than 15%.

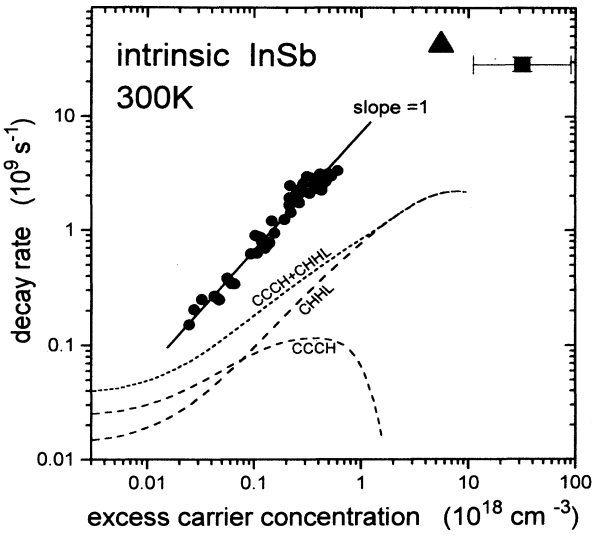

FIG. 5. InSb reciprocal lifetime dependence on the excess carrier concentration (●). Solid line, the best linear regression fit to our own data, gradient 1 (±0.04), corresponding to $\tau_{Aug}^{-1} = C_2 n$ with $C_2 = 7.4\times10^{-9}$ cm^{3}s^{-1}. ■, data from Ref. 13; △, data from Ref. 15. Dashed line, AR rates calculated using Beattie's (Ref. 12) mass-action coefficients for the CCCH and CHHL processes and the "dominant channel" occupation factors of Fig. 6.

Even at $n = 2.7\times10^{18}$ cm^3 the bulk plasma frequency was five times lower than our probe frequencies, so that the sample refractive-index and reflectivity changes due to the free-carrier plasma[19] were <1% and could be neglected. The refractive-index changes which occur due to the Burstein-Moss absorption changes in the interband absorption spectrum were computed using a Kramers-Kronig integral, and were also found to produce a negligible change in the sample reflectivity.

In common with previous measurements[8] at the time delays at which they were probed, the excess electron and hole distributions could be accurately characterized as spatially homogeneous Fermi-Dirac distributions thermalized to the lattice temperature. Only the electron and hole quasi-Fermi energies change as the carriers recombine. The maximum InSb epilayer temperature change due to the laser pulse was also calculated to be negligible (<8 K) and the single-valued relationship between carrier concentration and sample absorption

TABLE I. InSb parameters (Ref. 17) at 300 K.

Electron mass m_e (near $k=0$)	Heavy-hole mass m_{hh}	Light-hole mass m_{lh}	Band-gap energy E_g	C-band nonparabolicity parameter α $[E(1+\alpha E)=\hbar^2k^2/2m_e]$	Intrinsic carrier concentration	Refractive index n near $\lambda=4$ μm
$0.02m_0$	$0.45m_0$	$0.015m_0$	0.17 eV	0.65 eV^{-1}	2×10^{16} cm^{-3}	4.0

coefficient in our model makes it possible to extract carrier concentrations with high confidence from the differential transmission changes [(DTC) $=\ln(T/T_0)$] measured at various probe wavelengths.

From the measured decay of the DTC we computed the time-dependent carrier concentration $n(t)$ directly as a function of delay after excitation and Fig. 5 shows the result of this process, plotted as the reciprocal carrier lifetime $\tau^{-1}=(1/n)(dn/dt)$ versus excess carrier density n. The solid line represents the best fit and has a slope $=1(\pm 0.04)$. This confirms the "quadratic" rather than a "cubic" dependence of AR rate on carrier density: $dn/dt=-C_2n^2$, and regression yields $C_2=7.4(\pm 1.5)\times 10^{-9}\ \mathrm{cm^3\,s^{-1}}$.

IV. DISCUSSION

Calculating an *absolute* Auger lifetime for a particular semiconductor is complicated mainly by the difficulty in estimating the overlap integrals[7] for the cell-periodic components of the Bloch functions involved in the carrier-carrier Coulomb interaction. A very accurate band-structure model is required and, although the methods have been refined over the years, different theoretical techniques applied, for example, to the CCCH process in direct-gap materials,[20] still produce AR coefficient estimates which span two decades. Calculating the functional form of the carrier density dependence of the AR rate is, however, more straightforward.

We start with Beattie and Landsberg's "dominant channel" approach. Assuming that $\Delta n,\Delta p \gg n_0,p_0$ then, in the absence of strong screening, the number of AR events per second per unit volume R is simply proportional to the occupation factors of Eq. (5) and the inverse of the effective Auger lifetime τ_{Aug}^{-1} is equal to R/n. The 300-K density dependence of these occupation factors, computed within our nonparabolic band-structure model, is plotted in Fig. 6.

In the case of interest here, $1-f_n(k_2')$ is close to 1 for all but the highest concentrations, the hole statistics are Boltzmann-like, and $f_p(k_1')$ is proportional to p (and hence n). The electrons are at least partially degenerate though, so $f_n(k_1)$ has a sublinear n dependence. This situation gives an overall AR rate dependence $\tau_{\mathrm{Aug}}^{-1}\sim n^s$, where $0<s<2$ for the CCCH process (with $s\to 0$ as the electrons become highly degenerate) and $1<s<2$ for the CHHL process (with $s\to 1$ as the electrons become degenerate).

For $n\geq 10^{18}\ \mathrm{cm^{-3}}$ the Boltzmann approximation for the hole states starts to fail as well (Fig. 6) and the τ_{Aug}^{-1} versus n dependence slows down even further. At high carrier concentrations four-particle processes (e.g., second-order AR or phonon-assisted AR) may become significant, and these may act to increase the apparent value of the exponent s.

Although Beattie[12] calculates that the CCCH and CHHL processes give comparable AR rates when both carrier populations are nondegenerate, the rapid onset of electron degeneracy in our experimental regime leads to an early saturation ($s\to 0$) of the CCCH inverse lifetime while the CHHL inverse lifetime continues to rise with

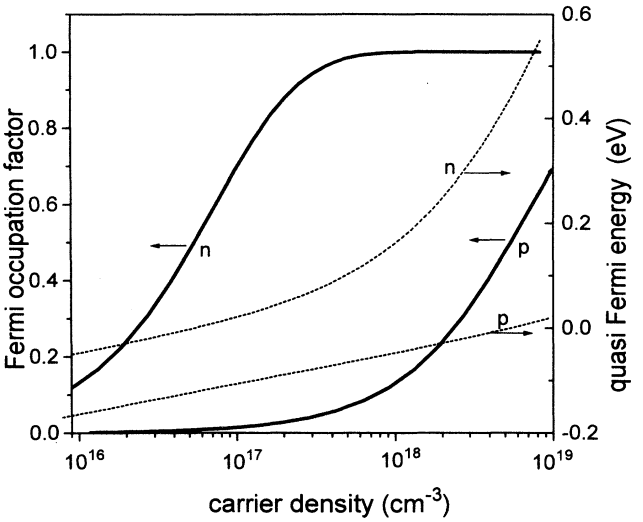

FIG. 6. Occupation probabilities for electrons and holes for the "dominant channel" AR states of Eqs. (1)–(4) and quasi-Fermi energies $E_F^n-E_c$ and $E_v-E_F^p$ as a function of carrier concentration. Using the parameters of Table I, Eqs. (1)–(4) give $E_{1,2}^{\mathrm{CCCH}}=0.29$ meV, $E_1^{\prime\mathrm{CHHL}}=0.061$ meV, $E_{1,2}^{\mathrm{CHHL}}=1.37$ meV, and $E_1^{\prime\mathrm{CCCH}}=6.64$ meV, and the different states in the same band have occupation factors which are, for practical purposes, the same on this plot.

$s=1$ as n increases. At very high electron concentrations the CCCH process almost ceases due to state filling of the final state E_2^{CCCH}. The dashed line in Fig. 5 is the Auger reciprocal lifetime calculated using Beattie's values for the CCCH and CHHL coefficients and the occupation factors for the "dominant channel" states of Fig. 6. The effect of the inverse (i.e., impact ionization) processes, significant at low excess-carrier concentrations, is also included.

Near $n=10^{18}\ \mathrm{cm^{-3}}$ the calculated (CCCH+CHHL) curve gives absolute Auger lifetimes some seven times larger than those we measure, but in view of the difficulties in the absolute Auger-lifetime calculation we regard this level of agreement as being acceptable. If we assume that Beattie is correct at least with respect to the *ratio* of the CCCH and CHHL C_3 coefficients, then the curves show that for $n>8\times 10^{16}\ \mathrm{cm^{-3}}$ the CHHL process is dominant and that the strong electron degeneracy significantly slows the AR rate at higher ($>10^{17}\ \mathrm{cm^{-3}}$) concentrations.

At $n=10^{17}\ \mathrm{cm^{-3}}$ the slope of the calculated curve is ~ 0.7, even smaller than that of our experimental data, and this may be the result of Beattie having underestimated the ratio of the CHHL and CCCH C_3 coefficients. The CHHL curve still has a slope near unity at this concentration, and increasing only Beattie's CHHL C_3 coefficient by a factor of ~ 7 would provide an excellent fit to our own data. Conversely, at higher carrier concentrations ($n>10^{18}\ \mathrm{cm^{-3}}$), the data of Fauchet[13] and Almazov *et al.*[15] indicate that the simple "dominant channel" model begins to fail and that higher-order pro-

cesses with a stronger n dependence start to become significant.

Our present observation of s being very close to unity is thus consistent with an AR mechanism dominated by "normal" (i.e., energy and wave-vector conserving) CHHL scattering events, in a situation where the electron statistics are strongly degenerate and the hole statistics are Boltzmann-like.

V. CONCLUDING REMARKS

By using a time-resolved midinfrared pump-probe transmission spectroscopy method, the direct time evolution of the excess carrier density has been studied in the carrier-density range $n=10^{16}-10^{18}$ cm^{-3} in high-quality thin films of intrinsic InSb. Because bimolecular recombination processes would have a density-independent effective lifetime under these degenerate conditions, the observed strong dependence of carrier lifetime on concentration implies that AR processes dominate in this regime. The AR rate was found to have a quadratic rather than a cubic dependence on carrier density, giving a reciprocal effective lifetime dependence $\tau_{\mathrm{Aug}}^{-1}=C_2 n$ with $C_2=7.4(\pm 1.5)\times 10^{-9}$ cm^{3}s^{-1}. This functional relationship is in good accordance with theoretical predictions[10] of Haug for degenerate semiconductors.

ACKNOWLEDGMENTS

We would like to thank the UK Engineering and Physical Sciences Research Council and the Royal Society of Great Britain for financial support for this work.

[1]A. R. Beattie and P. T. Landsberg, J. Phys. Chem. Solids **8**, 73 (1959).
[2]N. K. Dutta and R. K. Nelson, J. Appl. Phys. **53**, 74 (1982).
[3]E. Zeilinski, F. Keppler, S. Hauser, M. H. Pilkuhn, R. Sauer, and W. T. Tsang, IEEE J. Quantum Electron. **25**, 1407 (1989).
[4]H. Q. Le, G. W. Turner, S. J. Eglash, H. K. Choi, and D. A. Coppeta, Appl. Phys. Lett. **64**, 153 (1994).
[5]S. J. Eglash and H. K. Choi, Appl. Phys. Lett. **64**, 883 (1994).
[6]T. Ashley and C. T. Elliott, Semicond. Sci. Technol. **6**, C99 (1991).
[7]P. T. Landsberg, *Recombination in Semiconductors* (Cambridge University Press, Cambridge, England, 1991), pp. 220–312.
[8]K. L. Vodopyanov, H. Graener, C. C. Phillips, and T. J. Tate, Phys. Rev. B **46**, 13 194 (1992).
[9]M. E. Prise, M. R. Taghizadeh, S. D. Smith, and B. S. Wherrett, Appl. Phys. Lett. **45**, 652 (1984).
[10]A. Haug, Solid State Electron. **21**, 1281 (1978).
[11]H. Schweitzer, E. Zeilinski, S. Hauser, R. Stuber, M. H. Pilkuhn, G. Griffiths, H. Kroemer, and S. Subbanna, IEEE J. Quantum Electron. **23**, 977 (1987).
[12]A. R. Beattie, J. Phys. C **18**, 6501 (1985).
[13]P. M. Fauchet, Phys. Status Solidi A **58**, K211 (1980).
[14]P. M. Fauchet, Phys. Status Solidi B **110**, K11 (1982).
[15]L. A. Almazov, A. I. Liptuga, V. K. Malyutenko, and L. L. Fedorenko, Fiz. Tekh. Poluprovodn. **14**, 1940 (1980) [Sov. Phys. Semicond. **14**, 1154 (1980)].
[16]K. L. Vodopyanov, J. Opt. Soc. Am. B **10**, 1723 (1993).
[17]*Semiconductors. Intrinsic Properties of Group IV Elements and III-V, II-VI, and I-VII Compounds,* edited by O. Madelung, Landolt-Börnstein, New Series, Group III, Vol. 22, Pt. a (Springer-Verlag, Berlin, 1987), pp. 123–342.
[18]S. W. Kurnick and J. M. Powell, Phys. Rev. **116**, 597 (1959).
[19]R. H. Bube, *Electrons in Solids* (Academic, Boston, 1992), pp. 156–159.
[20]A. Haug, J. Phys. Chem. Solids **19**, 599 (1988).